Scripta Materialia 264 (2025) 116715

Contents lists available at ScienceDirect

Scripta Materialia

journal homepage: www.journals.elsevier.com/scripta-materialia

# 4D Observations of the initiation of abnormal grain growth in commercially pure Ni

Yi Wang [a], Zipeng Xu [a], Vivekanand Muralikrishnan [a], Joel B. Harley [b], Michael R. Tonks [b], Gregory S. Rohrer [1,a], Amanda R. Krause [a,*]

[a] Carnegie Mellon University, Pittsburgh PA, USA
[b] University of Florida, Gainesville, FL, USA

ARTICLE INFO

*Keywords:*
Nickel
Abnormal grain growth
Grain boundary energy
Grain boundary migration
X-ray diffraction contrast tomography

ABSTRACT

Abnormal grain growth (AGG), where a small fraction of grains grow faster than others, is critical to predict because it can significantly impact material properties. However, the mechanism behind AGG remains unclear. In this study, laboratory-based x-ray diffraction contrast tomography (LabDCT) is employed to non-destructively track the 3D microstructural evolution of high-purity nickel during the onset of AGG at 800 °C. The initial microstructure state is used to test hypothesized microstructure predictors of the initiation of AGG. The change in grain size was not related to the initial grain size or normalized integral mean curvature. Additionally, the grain boundary energy distributions of abnormal grains were indistinguishable from those of control groups exhibiting normal grain growth. However, the grains that later became abnormal exhibit large areas of asymmetric tilt boundaries that were previously found to be fast. This 3D microstructure dataset is useful to investigate new hypotheses for the initiation of AGG.

Abnormal grain growth (AGG), characterized by a small fraction of grains growing significantly faster than their neighbors, is a phenomenon of considerable importance for polycrystalline materials. This growth rate disparity between grains can result in heterogeneous mechanical properties and overall unreliable performance. Despite its significance, the mechanisms driving AGG remain unclear, creating challenges in predicting and controlling microstructural evolution of polycrystals.

Several theories and microstructure descriptors for predicting AGG in bulk polycrystals have been proposed. Residual stress or deformation history is often associated with the initiation of AGG in metals [1,2]. In the absence of such stored energy, AGG has been hypothesized to initiate in grains that are initially large in size, have many neighbors, or have high curvature [3]. However, Grest et al. used simulations to demonstrate that size differences alone cannot sustain AGG [4]. Instead, they found that abnormal grains maintained their growth advantage if their grain boundaries had a higher mobility or lower energy than the rest of the population. Since both GB energy and mobility depend on the GB character, defined by the misorientation and plane inclination, researchers suggest that particular GB types may initiate AGG [5–7]. Simulation studies also find that the probability of AGG increases with the likelihood of high mobility GBs neighboring one another [8]. This finding suggests that the population of particular GB types will influence the appearance of AGG. In FCC crystals, others have shown that Σ3 twin GBs, which are especially low energy, have a larger area fraction in microstructures with AGG compared to those exhibiting normal grain growth (NGG) [1].

However, these theories are difficult to validate due to a lack of time-resolved observations. Conventional microstructural characterization methods primarily rely on two-dimensional (2D) or destructive techniques [1,2,7,9,10], which provide insufficient information to identify predictors of grain growth behavior. For example, serial sectioning methods combined with electron backscattered diffraction (EBSD) provide 3D microstructural maps but are destructive, preventing grains and GBs from being tracked over time. Instead, microstructures are characterized before and after microstructure evolution on different samples, and thus, microstructural features of interest are compared statistically [11]. Furthermore, the boundaries associated with the grains that shrink

* Corresponding author.
*E-mail address:* amandakr@andrew.cmu.edu (A.R. Krause).
[1] Gregory S. Rohrer was an Editor of the journal during the review period of the article. To avoid a conflict of interest, Gregory S. Rohrer was blinded to the record and another editor processed this manuscript

https://doi.org/10.1016/j.scriptamat.2025.116715
Received 3 January 2025; Received in revised form 7 March 2025; Accepted 15 April 2025

away the fastest are preferentially removed from the analysis. In-situ EBSD can capture time-resolved information [12,13] but, without information about the GB position below the surface, such 2D characterization methods are insufficient for accurately describing GBs behavior in bulk polycrystals.

3D x-ray diffraction microscopy provides full microstructural maps non-destructively to interrogate grain growth in the same samples over time. Previously, such methods were used to investigate the role of particle pinning in AGG [14] and the role of curvature on GB velocity [15,16]. In this study, laboratory X-ray diffraction contrast tomography (LabDCT) was employed to obtain 3D microstructure maps of high-purity nickel polycrystals before and after annealing during which AGG occurred. The goal of this work is to identify microstructure features that predict the initiation of AGG. To that end, the initial grain size, normalized integral mean curvature, GB energy, and GB character are compared between grains exhibiting abnormal and normal growth behavior. As these features evolve during AGG, the study focuses on metrics that may indicate initiation of AGG and not how the growth advantage is maintained.

A grain growth study was performed with a sample cut from a cast nickel block with a purity of 99.99 % (Fisher Scientific, Waltham, USA). The block was cut into a 1 mm diameter cylindrical rod using electrical discharge machining to limit deformation. The sample was recrystallized in a tube furnace under flowing forming gas by heating to 600 °C at a rate of 20 °C/min. Upon reaching the set temperature, the furnace was cooled such that the tube dropped to 600 °C within 2 mins and to 200 °C within 17 min. The sample was then extracted to cool in air to room temperature. The grain growth study was completed at 800 °C for 5 mins using the same heating and cooling rates. Note that the heating rate effectively increases the time at elevated temperatures at which abnormal grain growth may occur.

LabDCT measurements were performed before and after annealing at 800 °C using a ZEISS CrystalCT with the flat panel detector and 250 mm × 750 mm aperture and beam stop. The sample was placed 11.6 mm from the source and 250 mm from the detector. The scans were collected using a voltage of 120 kV, power of 10 W, exposure time of 30 secs, and bin number of 2. The collected raw diffraction images were segmented and reconstructed using GrainMapper3D (Xnovo Technology ApS, DK) [17].

The sample height scanned by LabDCT was 2 mm both before and after the anneal, and it was reconstructed using cubic voxels with edge length of 5 μm. The microstructural maps were post-processed using Dream.3D [18], including segmentation using a misorientation threshold of 2°. Grains with fewer than 8 voxels or fewer than two neighbors were removed, and the surrounding grains were dilated using the minimum size and minimum number of neighbors filters, respectively. This post-processing method was chosen to preserve the original structure with minimal alterations. However, it does not reduce topological errors that are likely caused by noise in the data as is possible with other methods [19]. Dream.3D was also used to mesh the grain boundaries using quick surface mesh and Laplacian smoothing to characterize the GB planes. Grain registration was completed between scans by identifying grains with center-of-mass distances <50 μm and misorientations below 0.5°. Grains with multiple pairs were removed from analysis due to uncertainty. For large grains found after annealing that were not tracked using this process, threshold parameters were adjusted. Overall, 6282 of the 19,799 and 7958 grains in the first and second scans, respectively, were tracked. Grains with an initial size of <20 μm were excluded from the analysis due to the resolution limitation. All grains touching the sample surface or the top and bottom of the scanned volume were removed from the analysis, resulting in 3824 tracked grains. The integral mean curvature of the GB is measured by the innie-outie method on a voxelated grid structure as described by [20,21]. The normalized integral mean curvature is calculated by using the sum of the integral mean curvature of all GBs related to the grain (thus, the net interface curvatures of the grain faces, excluding curvatures due to the triple junctions or quadruple points) divided by the grain radius, and is a dimensionless quantity. Here, a positive and negative integral mean curvature indicates a concave and convex surface, respectively. GB energy is calculated using the function proposed by Bulatov, Reed, and Kumar based on the full five crystallographic degrees of freedom (i.e., misorientation and inclination) [22].

Abnormal grains were identified by the change in grain size (ΔG), which is the difference in spherical equivalent grain diameters measured before and after heat treatment. The average grain size of all grains (including untracked grains but not grains smaller than 20 μm) increased from 47 μm to 56 μm (9 μm increase). An abnormal grain is, thus, defined as one that had an increase in grain size 5 times larger than the average value ($\Delta G > 50$ μm), and 84 grains were identified. A control group of normal growing grains ($\Delta G < 30$ μm) was selected that contains the same number of grains and a similar initial average size as the abnormal grain population. Additionally, it was ensured that these normal grains grew ($\Delta G > 0$) and did not neighbor any abnormal grains. Fig. 1a illustrates the microstructure before and after annealing, highlighting the presence of both normal and abnormal grains. The abnormal grains and control group are shown in Fig. 1b and 1c, respectively, before (black) and after (colored according to grain orientation) grain growth. Fig. 1d shows that abnormal and control groups are of similar size in the initial microstructure and randomly distributed throughout the volume. (Note that other criteria used to evaluate AGG, such as final

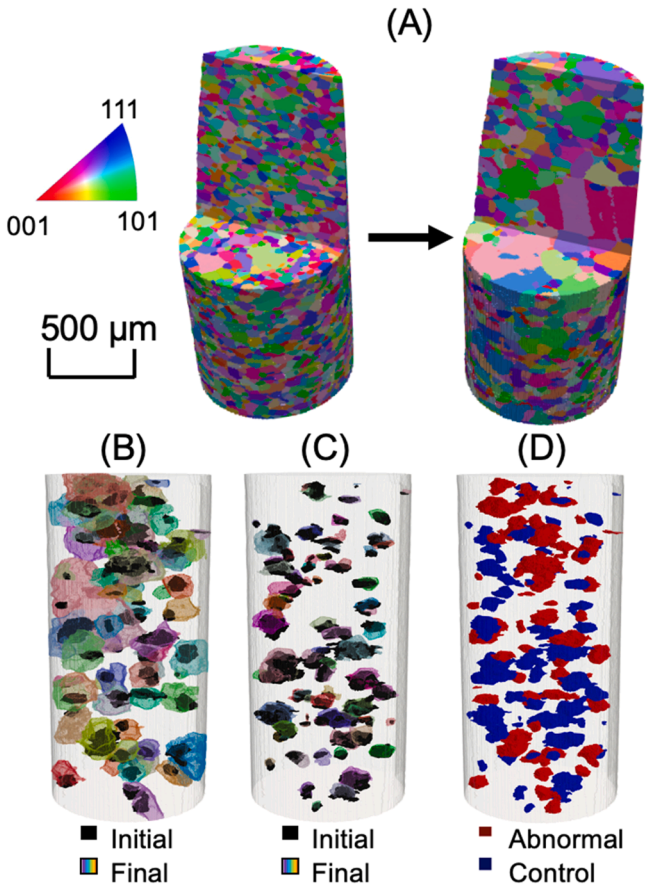


**Fig. 1.** Visualization in 3D of Ni microstructure and select grains mapped by LabDCT. (A) Full 3D microstructure before and after grain growth at 800 °C. (B) Map of the identified abnormal grains and (C) selected control group (exhibiting NGG) before (solid black) and after growth (transparent color). (D) Map of both the abnormal (red) and control groups (blue) in the initial state, demonstrating that their spatial distributions are uniform and similar. Except otherwise noted, grains are colored based on the provided inverse pole figure key according to their orientation with respect to the long axis of the cylindrical sample.

grain size or ΔG normalized by initial grain size, did not change the results significantly and are discussed in the supplemental information.)

Table 1 reports the number of grains, their average size before and after annealing, and the total number of grain boundaries used in the analysis for the classified abnormal grains, control group and all tracked grains. Note that for all tracked grains, the average ΔG is only 1 μm whereas it was reported above as 9 μm for all grains. This difference is due to many, small untracked grains that, when included, significantly reduce the average initial grain size. Table 1 also shows that the average ΔG for identified abnormal grains is an order of magnitude greater than the control group, which represents a threshold previously associated with "extreme" AGG by [7]. The "extreme" nature of this growth is exemplified by the change in volume (ΔV).

The change in grain size does not correlate with the initial grain size nor the normalized integral mean curvature as shown in Fig. 2. These results agree with previous observations of Ni exhibiting NGG [23]. The lack of correlation is seen for all grains, including abnormal grains (represented in red in Fig. 2). In particular, large grains or those with large absolute curvatures do not have a growth advantage as previously speculated by [16,24–26]. Furthermore, these metrics do not differentiate abnormal grains from the normal population.

Fig. 2c compares the grain size distributions of the abnormal grains to all tracked grains and the control group. The abnormal grain size population skews larger than the general population. Despite this difference, grain size cannot be used as an indicator of abnormal growth because the number of normally growing grains exceeds that of abnormal grains for every size range. (Refer to the histogram in the supplementary information for more details.) Other potential microstructural features of interest to AGG may be affected by the initial grain size distribution. To eliminate the grain size effect when comparing other potential indicators of AGG, abnormal grains are compared to a control group with an initially similar grain size distribution as discussed above. The control group is represented in blue in Fig. 2 and details can be found in Table 1.

Fig. 2d shows that abnormal grains are more likely to have a negative integral mean curvature (i.e., concave) than a positive one (i.e., convex), which agrees with predictions for the preferred growth of concave grains. However, this same trend is seen with the control group, reflecting the correlation between grain size and integral mean curvature rather than any trend between grain growth *rate* and integral mean curvature. Notably, some abnormal grains (31 grains, 37 %) have a positive integral mean curvature, indicating that they are initially convex and grow in the direction opposite of their center of curvature. The initial grain boundaries associated with abnormal grains do not exist after abnormal growth, limiting the ability to assess whether individual interfaces moved away from their center of curvature.

Fig. 3a shows the GB energy distributions associated with the abnormal and control groups, indicating no obvious difference in the initial state. Therefore, abnormal grains are not associated with GBs of uniquely high or low energy. An additional test investigating the GB energy difference between it and its direct neighbors did not distinguish abnormal and normal grains (see supplementary materials).

Previously, others speculated that AGG may promote the expansion of Σ3 twin boundaries to effectively reduce the total energy of the GB network [27]. The presence of Σ3 ([1 1 1]/60°) twin boundaries was investigated here, and no significant difference in their population or area density could be found to differentiate the abnormal grains and control group, as shown in Fig. 3b.

Some differences are found when comparing the initial GB plane distribution of Σ3 GB between abnormal and normal grains. Fig. 4a illustrates the relative plane population for Σ3 GBs. The (111) direction, which corresponds to the coherent twin boundary, exhibits the highest relative area, quantified by as multiples of a random distribution (MRD). This finding aligns with previous results [16], supporting the significant prevalence of coherent twin boundaries in the FCC Ni. Figs. 4b and 4c illustrate the plane distribution of Σ3 GB associated with abnormal grains and the control group, respectively, in which notably large relative areas appear near (111) in both figures. However, Figs. 4b and 4c show differences along the zone corresponding to the asymmetric tilt boundaries. For example, the abnormal grain-related Σ3 GBs have greater relative area near the$(\bar{1}11)$ poles (including $(\bar{1}\bar{1}1)$ and $(1\bar{1}1)$, which are equivalent and represented by squares) and their complementary planes, which are near the (100) (represented by pentagons), than found for the normal grains. Interestingly, these Σ3 GBs are asymmetric tilt boundaries that have previously been identified as high velocity in a previous Ni study exhibiting NGG [16]. Due to the amount of growth exhibited between measurements, the velocity of these grain boundaries cannot be conclusively measured.

It is notable that the control group does not have a local maximum at the $(\bar{1}11)$ (asymmetric tilt) for Σ3 GBs like the abnormal grains in this study. The GB plane distribution may vary slightly depending on which grains are selected for the control group. This study randomly sampled other normal grains that fit the criteria listed above to test the reliability of the experimental results. Some groups exhibited higher relative areas in the $(\bar{1}11)$ direction, while others showed the opposite trend. However, none of the NGG groups exhibited a local maximum like seen for the abnormal grains. For details, please refer to the supplementary materials.

The higher relative population of these Σ3 $(\bar{1}11)$ asymmetric tilt GBs on abnormal grains may support their growth advantage initially. However, it is unclear how the growth of these grains is maintained after their neighbors are consumed, effectively replacing the GB. Furthermore, their presence is not always associated with AGG such that they alone are not a predictor of AGG.

In this study, LabDCT microstructure maps were used to evaluate the relationship between the initiation of AGG and various grain and grain boundary features. No correlations were found between initial grain size and normalized integral mean curvature and the change in grain size (ΔG) for normal or abnormal grains. Additionally, none of the features were predictive of AGG. The GB energy and Σ3 area ratio distributions of the precursors of abnormal grains were indistinguishable from control groups, which had the same initial average grain size but exhibited NGG. This study found a high population of asymmetric Σ3 tilt boundaries associated with abnormal grains, which were found to be fast in a previous study. This finding suggests that while GB geometry and energy in the initial precursor grains cannot predict AGG, the grains that later became abnormal had large areas of fast GBs in the initial state. However, it is unclear how these boundaries maintain a growth advantage as their neighbors are annihilated or why other grains that contain these boundaries do not grow abnormally fast. Additional experiments, such as residual strain measurements and elemental analysis at the GBs, are necessary to rule out other potential factors influencing AGG. More or finer time steps will allow for investigations of the persistence of AGG to test hypotheses related to the evolution of topological events as

**Table 1**
The number of grains, average grain sizes (G) before and after growth, average change in grain sizes (ΔG) and volumes (ΔV) during growth at 800 °C, and number of GBs analyzed in this study for all tracked grains, classified abnormal grains, and the control group.

| Groups | Number of grains | Average Initial Size (μm) | Average Final Size (μm) | Average ΔG (μm) | Average ΔV ($\mu m^3$) | Number of GBs |
|---|---|---|---|---|---|---|
| Abnormal | 84 | 79 | 162 | 83 | 2770,898 | 2696 |
| Normal-Control | 84 | 77 | 88 | 11 | 161,531 | 2660 |
| All tracked | 3824 | 58 | 60 | 2 | 84,836 | 57,393 |

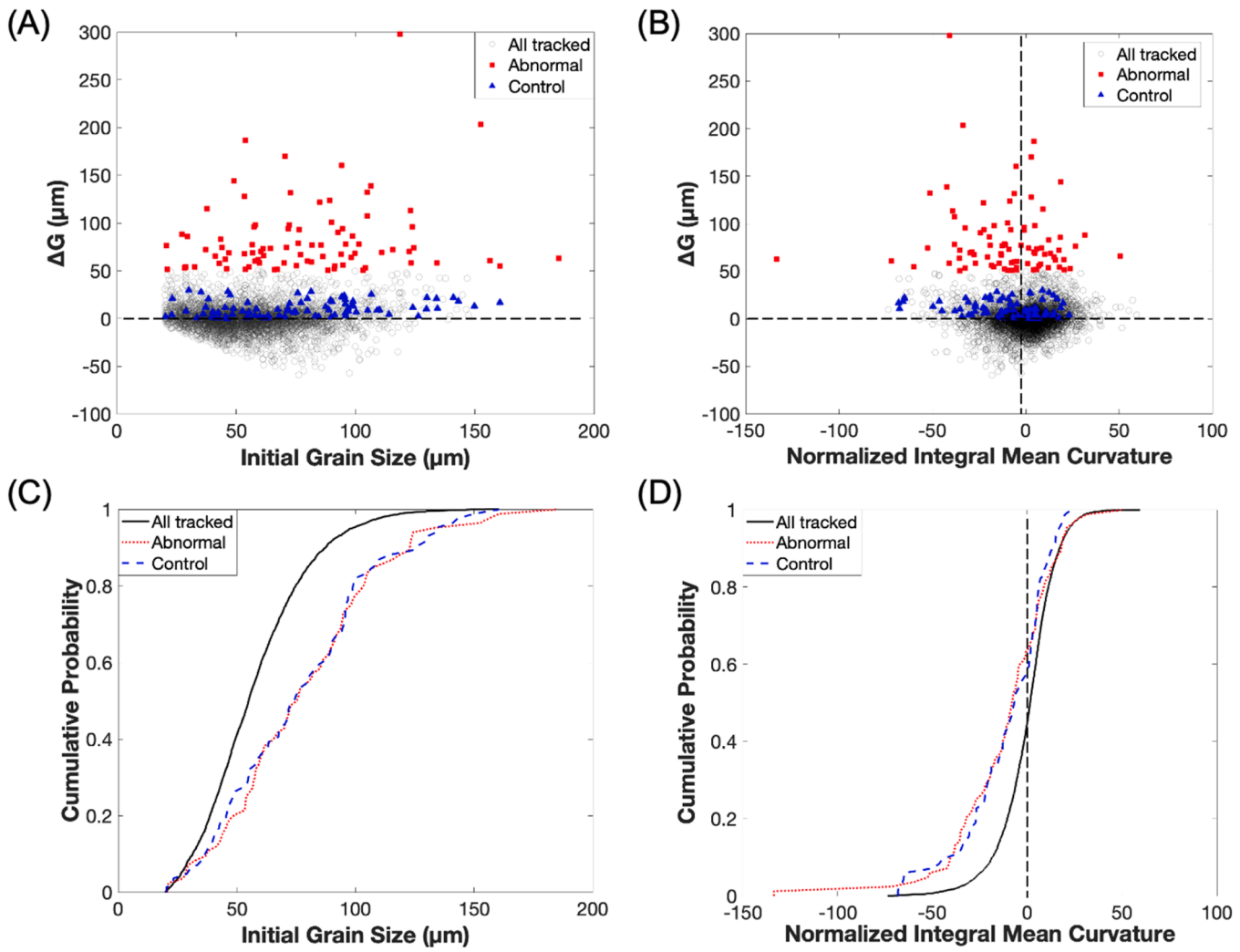


**Fig. 2.** The relationships between grain size change and the initial size and normalized integral mean curvature. All tracked grains are included, and the abnormal grains and control group are shown in red and blue, respectively. Scatter plots of the (A) grain size change and initial size and (B) grain size change and the normalized integral mean curvature. Cumulative distribution plot of the (C) grain size and (D) normalized integral mean curvature for the grains before grain growth.

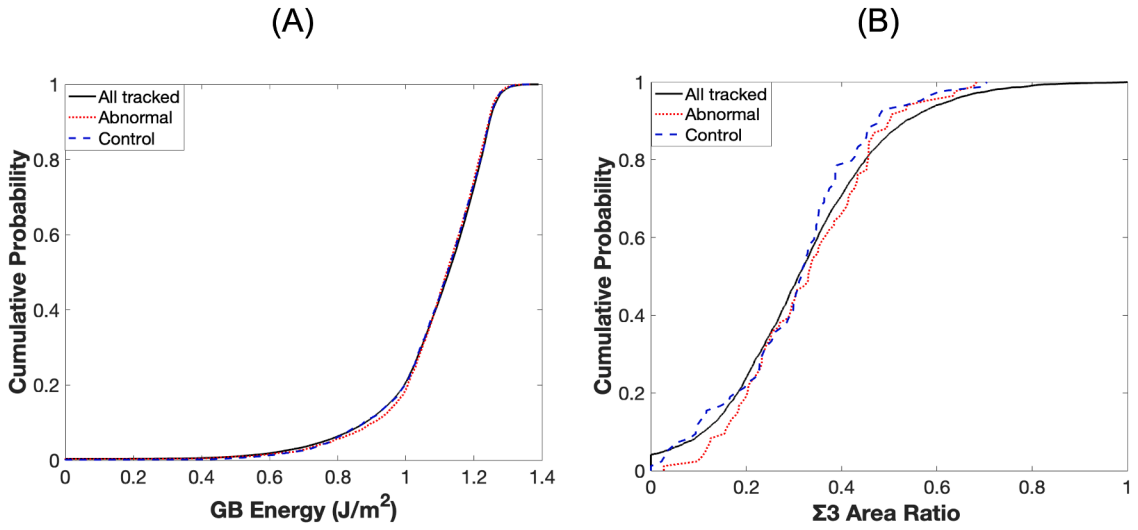


**Fig. 3.** Cumulative distribution plots of initial (A) GB energy and (B) Σ3 area ratio for all tracked grains (black), abnormal grains (red), and the normal control group (blue).

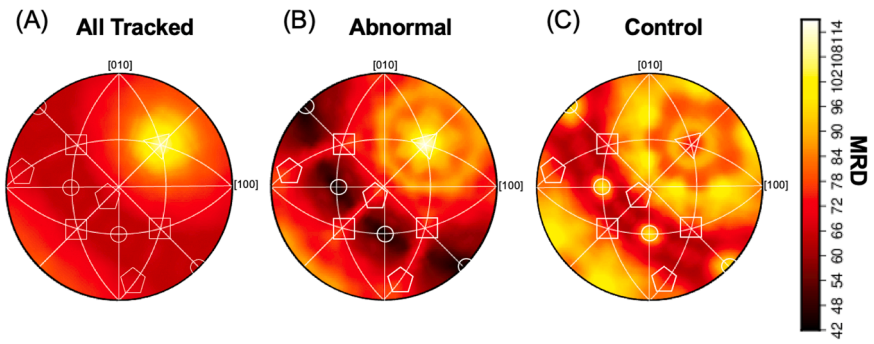


**Fig. 4.** The relative areas (measured by multiple of random distribution, MRD) of initial Σ3 GBs associated with (A) all tracked grains, (B) abnormal grains, and (C) the control group. All plots are stereographic projections along the [001] axis. The Σ3 GB plane inclinations indicated by triangles, circles, squares and pentagons are the (111), (1$\bar{1}$0), ($\bar{1}$11), and their complementary plane that is close to (100), respectively.

proposed by [28].

## CRediT authorship contribution statement

**Yi Wang:** Writing – original draft, Methodology, Investigation, Formal analysis. **Zipeng Xu:** Validation, Investigation. **Vivekanand Muralikrishnan:** Investigation. **Joel B. Harley:** Writing – review & editing, Funding acquisition. **Michael R. Tonks:** Writing – review & editing, Funding acquisition. **Gregory S. Rohrer:** Writing – review & editing, Supervision. **Amanda R. Krause:** Writing – review & editing, Supervision, Project administration, Funding acquisition, Conceptualization.

## Declaration of competing interest

The author Gregory S. Rohrer is Coordinating Editor for Scripta Materialia and was not involved in the editorial review or the decision to publish this article.

## Acknowledgements

This research was supported by the U.S. Department of Energy, Office of Science, USA, under Grant No DE-SC0023380. Z.X. and G.S.R. were supported by the National Science Foundation under DMREF Grant No. 2118945. The authors acknowledge use of the Materials Characterization Facility at Carnegie Mellon University supported by grant MCF-677785.

## Supplementary materials

Supplementary material associated with this article can be found, in the online version, at doi:10.1016/j.scriptamat.2025.116715.

## References

[1] S. Qiao, S. Liu, N. Li, X. Gao, X. Wen, F. Wang, C. Yuan, Abnormal grain growth in the Ni-based wrought superalloy GH4698 bar during heat treatment, J. Mater. Res. Technol. 30 (2024) 6563–6575, https://doi.org/10.1016/j.jmrt.2024.05.089.
[2] O.D. Underwood, J.D. Madison, G.B. Thompson, Emergence and progression of abnormal grain growth in minimally strained nickel-200, Metals. 7 (2017) 334, https://doi.org/10.3390/met7090334.
[3] J.E. Taylor, J.W. Cahn, C.A. Handwerker, Overview No. 98 I—Geometric models of crystal growth, Acta Metall. Mater. 40 (1992) 1443–1474, https://doi.org/10.1016/0956-7151(92)90090-2.
[4] G.S. Grest, M.P. Anderson, D.J. Srolovitz, A.D. Rollett, Abnormal grain growth in three dimensions, Scr. Metall. Mater. 24 (1990) 661–665, https://doi.org/10.1016/0956-716X(90)90219-7.
[5] D.G. Brandon, The structure of high-angle grain boundaries, Acta Metall 14 (1966) 1479–1484, https://doi.org/10.1016/0001-6160(66)90168-4.
[6] W.T. Read, W. Shockley, Dislocation models of crystal grain boundaries, Phys. Rev. 78 (1950) 275–289, https://doi.org/10.1103/PhysRev.78.275.
[7] C.E. Krill, E.A. Holm, J.M. Dake, R. Cohn, K. Holíková, F. Andorfer, Extreme abnormal grain growth: connecting mechanisms to microstructural outcomes, Annu Rev. Mater. Res. 53 (2023) 319–345, https://doi.org/10.1146/annurev-matsci-080921-091647.
[8] W.E. Frazier, G.S. Rohrer, A.D. Rollett, Abnormal grain growth in the Potts model incorporating grain boundary complexion transitions that increase the mobility of individual boundaries, Acta Mater. 96 (2015) 390–398, https://doi.org/10.1016/j.actamat.2015.06.033.
[9] S.B. Lee, N.M. Hwang, D.Y. Yoon, M.F. Henry, Grain boundary faceting and abnormal grain growth in nickel, Metall. Mater. Trans. A. 31 (2000) 985–994, https://doi.org/10.1007/s11661-000-0040-3.
[10] D.J. Jensen, Y. Zhang, Nucleation of recrystallization, J. Phys. Conf. Ser. 2635 (2023) 012001, https://doi.org/10.1088/1742-6596/2635/1/012001.
[11] J. Greiser, P. Müllner, E. Arzt, Abnormal growth of "giant" grains in silver thin films, Acta Mater. 49 (2001) 1041–1050, https://doi.org/10.1016/S1359-6454(00)00372-4.
[12] S. Takajo, C.C. Merriman, S.C. Vogel, D.P. Field, In-situ EBSD study on the cube texture evolution in 3 wt % Si steel complemented by ex-situ EBSD experiment — From nucleation to grain growth, Acta Mater. 166 (2019) 100–112, https://doi.org/10.1016/j.actamat.2018.11.054.
[13] N.A. Pedrazas, T.E. Buchheit, E.A. Holm, E.M. Taleff, Dynamic abnormal grain growth in tantalum, Mater. Sci. Eng. A 610 (2014) 76–84, https://doi.org/10.1016/j.msea.2014.05.031.
[14] N. Lu, J. Kang, N. Senabulya, R. Keinan, N. Gueninchault, A.J. Shahani, Dynamics of particle-assisted abnormal grain growth revealed through integrated three-dimensional microanalysis, Acta Mater. 195 (2020) 1–12, https://doi.org/10.1016/j.actamat.2020.04.049.
[15] V. Muralikrishnan, H. Liu, L. Yang, B. Conry, C.J. Marvel, M.P. Harmer, G. S. Rohrer, M.R. Tonks, R.M. Suter, C.E. Krill, A.R. Krause, Observations of unexpected grain boundary migration in SrTiO3, Scr. Mater. 222 (2023) 115055, https://doi.org/10.1016/j.scriptamat.2022.115055.
[16] A. Bhattacharya, Y.-F. Shen, C.M. Hefferan, S.F. Li, J. Lind, R.M. Suter, C.E. Krill, G. S. Rohrer, Grain boundary velocity and curvature are not correlated in Ni polycrystals, Science (1979) 374 (2021) 189–193, https://doi.org/10.1126/science.abj3210.
[17] A. Lindkvist, H. Fang, D.Juul Jensen, Y. Zhang, Optimizing laboratory X-ray diffraction contrast tomography for grain structure characterization of pure iron, J. Appl. Crystallogr. 54 (2021) 99–110, https://doi.org/10.1107/S1600576720014673.
[18] M.A. Groeber, M.A. Jackson, DREAM.3D: a digital representation environment for the analysis of microstructure in 3D, integrating mater, Manuf. Innov. 3 (2014) 56–72, https://doi.org/10.1186/2193-9772-3-5.
[19] M. Chlupsa, Z. Croft, K. Thornton, A.J. Shahani, Enhancing polycrystalline-microstructure reconstruction from X-ray diffraction microscopy with phase-field post-processing, Scr. Mater. 252 (2024) 116228, https://doi.org/10.1016/j.scriptamat.2024.116228.
[20] D.J. Rowenhorst, A.C. Lewis, G. Spanos, Three-dimensional analysis of grain topology and interface curvature in a β-titanium alloy, Acta Mater. 58 (2010) 5511–5519, https://doi.org/10.1016/j.actamat.2010.06.030.
[21] B. Patterson, R. DeHoff, C. Sahi, J. Sun, J. Oddershede, F. Bachmann, E. Lauridsen, D.J. Jensen, Integral mean curvature analysis of 3D grain growth: linearity of dV/dt and grain volume, IOP. Conf. Ser. Mater. Sci. Eng. 580 (2019) 012020, https://doi.org/10.1088/1757-899X/580/1/012020.
[22] V.V. Bulatov, B.W. Reed, M. Kumar, Grain boundary energy function for fcc metals, Acta Mater. 65 (2014) 161–175, https://doi.org/10.1016/j.actamat.2013.10.057.
[23] A. Bhattacharya, Y.-F. Shen, C.M. Hefferan, S.F. Li, J. Lind, R.M. Suter, G.S. Rohrer, Three-dimensional observations of grain volume changes during annealing of polycrystalline Ni, Acta Mater. 167 (2019) 40–50, https://doi.org/10.1016/j.actamat.2019.01.022.
[24] G. Gottstein, D.A. Molodov, L.S. Shvindlerman, D.J. Srolovitz, M. Winning, Grain boundary migration: misorientation dependence, Curr. Opin. Solid. State Mater. Sci. 5 (2001) 9–14, https://doi.org/10.1016/S1359-0286(00)00030-9.
[25] M. Upmanyu, R.W. Smith, D.J. Srolovitz, Atomistic simulation of curvature driven grain boundary migration, Interface Sci 6 (1998) 41–58, https://doi.org/10.1023/A:1008608418845.

[26] G. Gottstein, D.A. Molodov, L.S. Shvindlerman, Grain-boundary energy and mobility, in: Metals Process Simulation, ASM International (2010) 67–91, https://doi.org/10.31399/asm.hb.v22b.a0005507.
[27] B. Lin, Y. Jin, C.M. Hefferan, S.F. Li, J. Lind, R.M. Suter, M. Bernacki, N. Bozzolo, A. D. Rollett, G.S. Rohrer, Observation of annealing twin nucleation at triple lines in nickel during grain growth, Acta Mater. 99 (2015) 63–68, https://doi.org/10.1016/j.actamat.2015.07.041.
[28] A.J. Shahani, K. Walter, J. Zhang, W. Ludwig, D.Juul Jensen, Y. Zhang, The evolution of intergranular networks during grain growth and its effect on percolation behavior, Acta Mater. 274 (2024) 119987, https://doi.org/10.1016/j.actamat.2024.119987.

**Abnormal Grain Classification**

AGG were also classified by normalized size change (i.e., change in grain size divided by initial grain size, $\Delta G/G_0$) to test whether different classifications changed the results. The average $\Delta G/G_0$ is 0.3 for tracked grains, and the threshold for abnormal grains was selected to be five times the average (1.5). Only grains with an initial size greater than 20 µm were considered, resulting in 32 identified abnormal grains as shown in Fig. S1 and described in Table S1. The same analysis as presented in the main text was completed with no significant differences in the results. The change in grain size does not correlate with the initial grain size nor the normalized integral mean curvature, as shown in Fig. S2. The GBs associated with abnormal grains are not uniquely higher or lower in energy than the rest of the population, as shown in Fig. S3a.

Table S1: The number of grains, average grain sizes (G) before and after growth, normalized average change in grain sizes ($\Delta G/ G_0$) and average change in volumes ($\Delta V$) during growth at 800°C, and number of GBs analyzed in this study for all tracked grains, classified abnormal grains, and the control group.

| | Number of grains | Average initial size (µm) | Average final size (µm) | $\Delta G/G_0$ | Average $\Delta V$ ($\mu m^3$) | Number of GBs |
|---|---|---|---|---|---|---|
| Abnormal | 32 | 39 | 132 | 2.4 | 2,956,625 | 392 |
| Control | 32 | 40 | 46 | 0.15 | 40,840 | 363 |

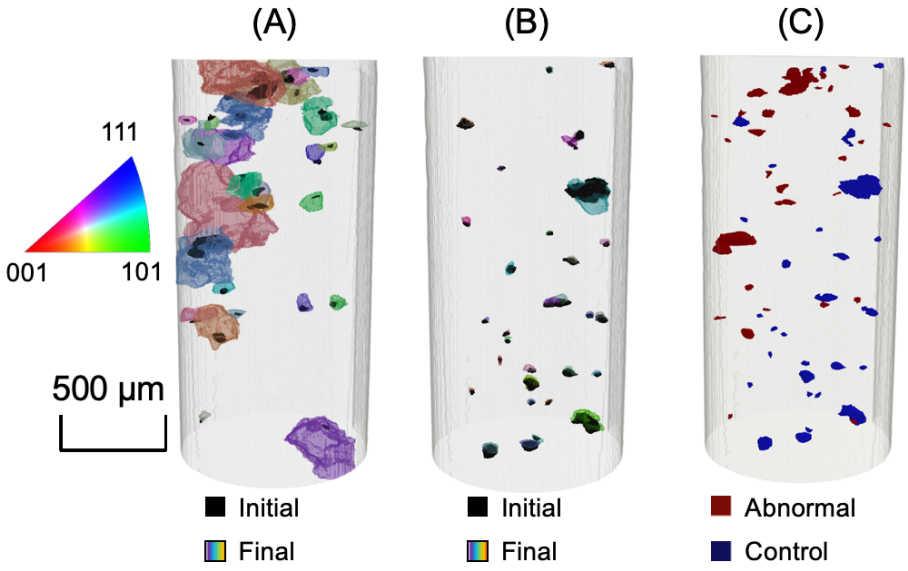


Figure S1: Visualization in 3D of Ni microstructure and select grains mapped by LabDCT. Map of the (A) identified abnormal grains and (B) selected control group (exhibiting NGG) before (solid black) and after growth (transparent color). (C) Map of both the abnormal (red) and control groups (blue) in the initial state, demonstrating that their spatial distributions are uniform and similar. Except otherwise noted, grains are

colored based on the provided inverse pole figure key according to their orientation with respect to the long axis of the cylindrical sample.

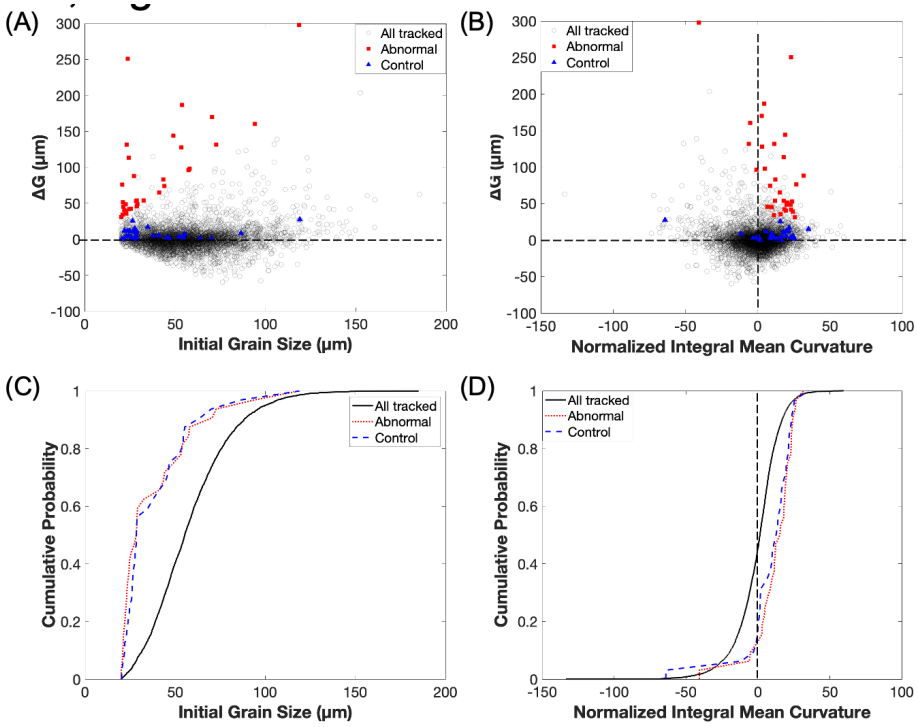


Figure S2: The relationships between grain size change and the initial size and normalized integral mean curvature. All tracked grains are included, and the abnormal grains and control group are shown in red and blue, respectively. Scatter plots of the (A) grain size change and initial size and (B) grain size change and the normalized integral mean curvature. Cumulative distribution plot of the (C) grain size and (D) normalized integral mean curvature for the grains before grain growth.

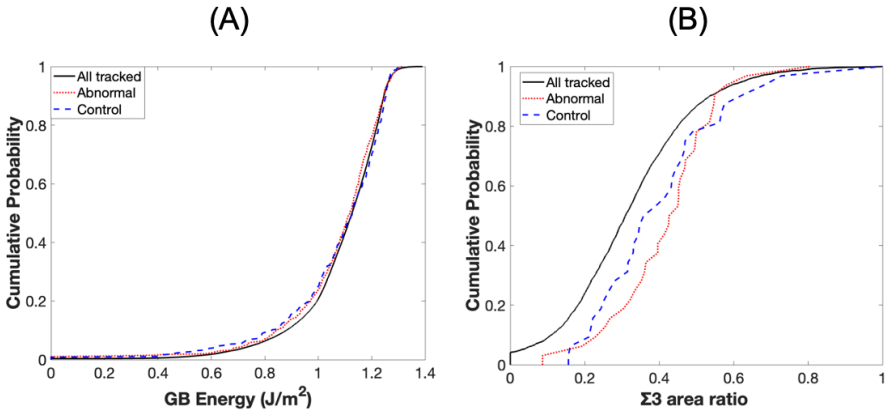


Figure S3: Cumulative distribution plots of (A) GB energy and (B) Σ3 area ratio for all tracked grains (black), abnormal grains (red), and the normal control group (blue).

**Difference in GB Energy**

The local driving force for GB motion has been recently hypothesized as the difference in energy between neighboring GBs [26], such that a lower energy GB will want to expand at the expense of its higher energy neighbors. To test if abnormal grains initially have lower energy GBs than their direct neighbors, the energy difference ($\Delta\gamma$) between neighboring GBs at every triple line was calculated as illustrated in Fig. S4. At each triple line of an abnormal grain with two normal grains, the energy of the two GBs between the abnormal grain and each neighboring grain were averaged together ($\overline{\gamma_A}$) and subtracted from the energy of the GB between the normal grains ($\gamma_N$). (For the control group, the $\Delta\gamma$ is the difference between the average of the selected grain's GBs and the neighboring GB at each triple junction, effectively substituting the abnormal grain for a grain from the control group.) The $\Delta\gamma$ distributions for the abnormal and control groups are nearly identical (Fig. S4), suggesting that one cannot predict AGG from GB energy or direct differences with their neighbors.

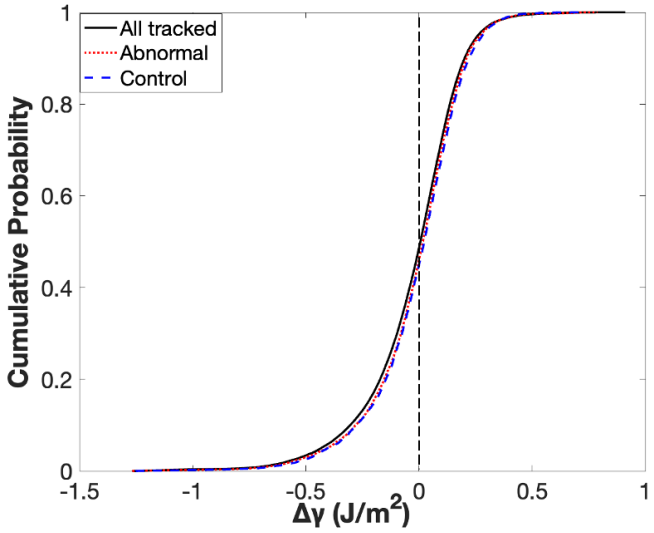


Figure S4: Cumulative distribution plot of the initial difference in GB energy at triple lines for the abnormal grains (red) and normal control group (blue).

**Grain Size Distribution**

Figure S5 is a histogram showing the initial grain size distribution for all tracked grains, abnormal grains, and the control group. Note that the abnormal and control groups are those presented in Table 1. The abnormal grains are a small subset of the entire population such that more normal growing grains are found for every size range. Note that the abnormal grains span the entire grain size population, including 17 grains with spherical-equivalent diameters smaller than 50 μm. The number of normally growing grains exceeds that of abnormal grains for every size range. For example, 49 normal grains and 10 abnormal grains are observed with an initial size greater than 120 μm.

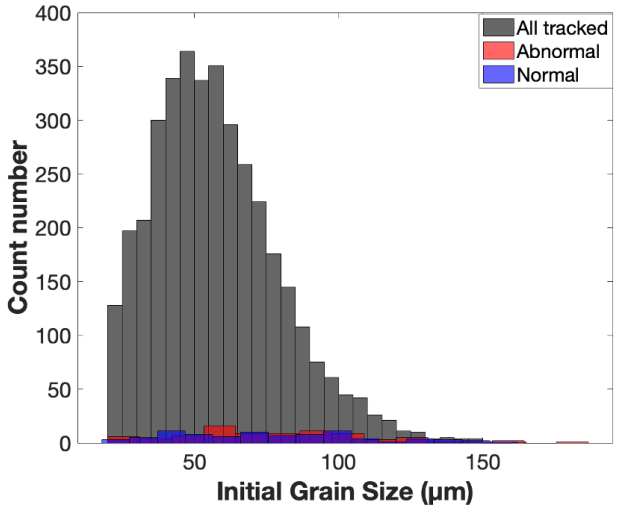


Figure S5: Histogram showing the grain size distribution for all tracked grains, abnormal grains and the normal control group.

**Sampling Different Control Groups**

To assess whether the grains in the control group biased the results, different grains were sampled to form five new control groups. Table S2 lists the details for five different control groups sampled with the same criteria as described in the main text. Figure S6 shows that the grains in all tested control groups show the same initial grain size distribution and normalized integral mean curvature, which is similar to the abnormal grains as classified by ΔG. Figure S7 shows that the distribution of GB energy and Δγ are also indistinguishable between the different control groups and the abnormal grains as classified by ΔG. The GB character distribution for Σ3 GBs is sensitive to the grains selected in the control group as shown in Fig. S8. However, no control group resembles that of the abnormal grains shown in S8A.

Table S2: The number of grains, average grain sizes (G) before and after growth, average change in grain sizes (ΔG) and volumes (ΔV) during growth at 800°C, and number of GBs analyzed for the five control groups.

| | Number of grains | Initial size (μm) | Final size (μm) | ΔG (μm) | Average ΔV ($\mu m^3$) | Number of GBs |
|---|---|---|---|---|---|---|
| Control 1 | 84 | 75 | 84 | 9 | 131,683 | 2557 |
| Control 2 | 84 | 76 | 85 | 9 | 122,474 | 2528 |
| Control 3 | 84 | 76 | 84 | 8 | 125,885 | 2540 |
| Control 4 | 84 | 74 | 84 | 10 | 134,772 | 2489 |
| Control 5 | 84 | 76 | 85 | 9 | 127,443 | 2555 |

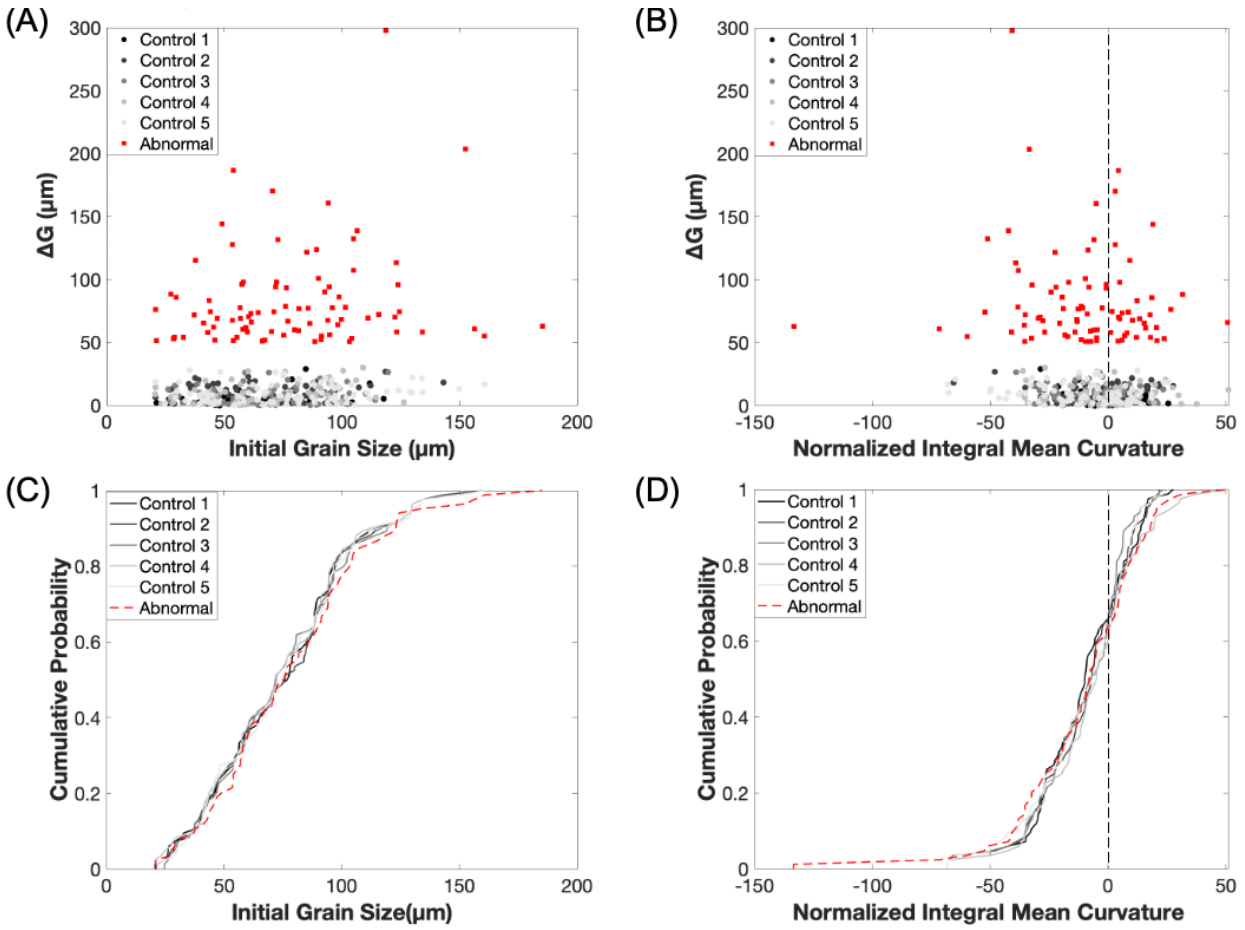


Figure S6: The relationships between grain size change and the initial size and normalized integral mean curvature for abnormal grains (red) and each of the control groups (grayscale). Scatter plots of the (A) grain size change and initial size and (B) grain size change and the normalized integral mean curvature. Cumulative distribution plot of the (C) grain size and (D) normalized integral mean curvature for the grains before grain growth.

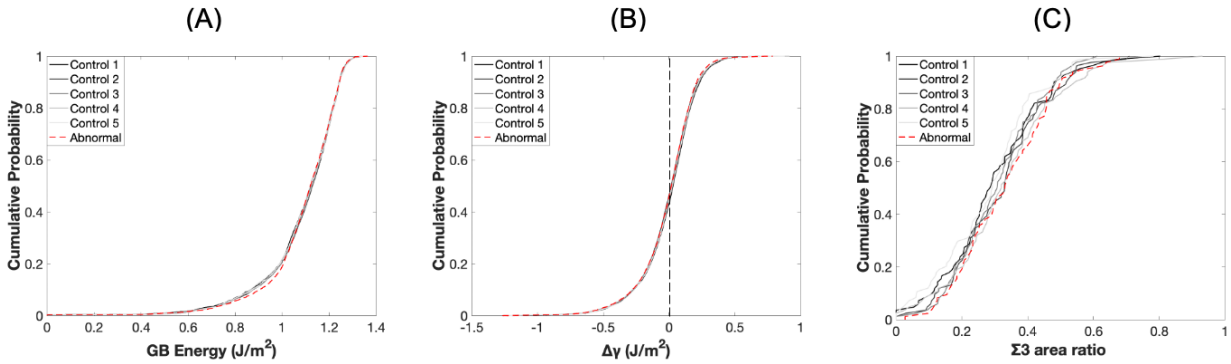

Figure S7: Cumulative distribution plots of (A) GB energy, (B) difference in GB energy at triple lines, and (C) Σ3 area ratio for abnormal grains (red), and each of the five control groups (grayscale).

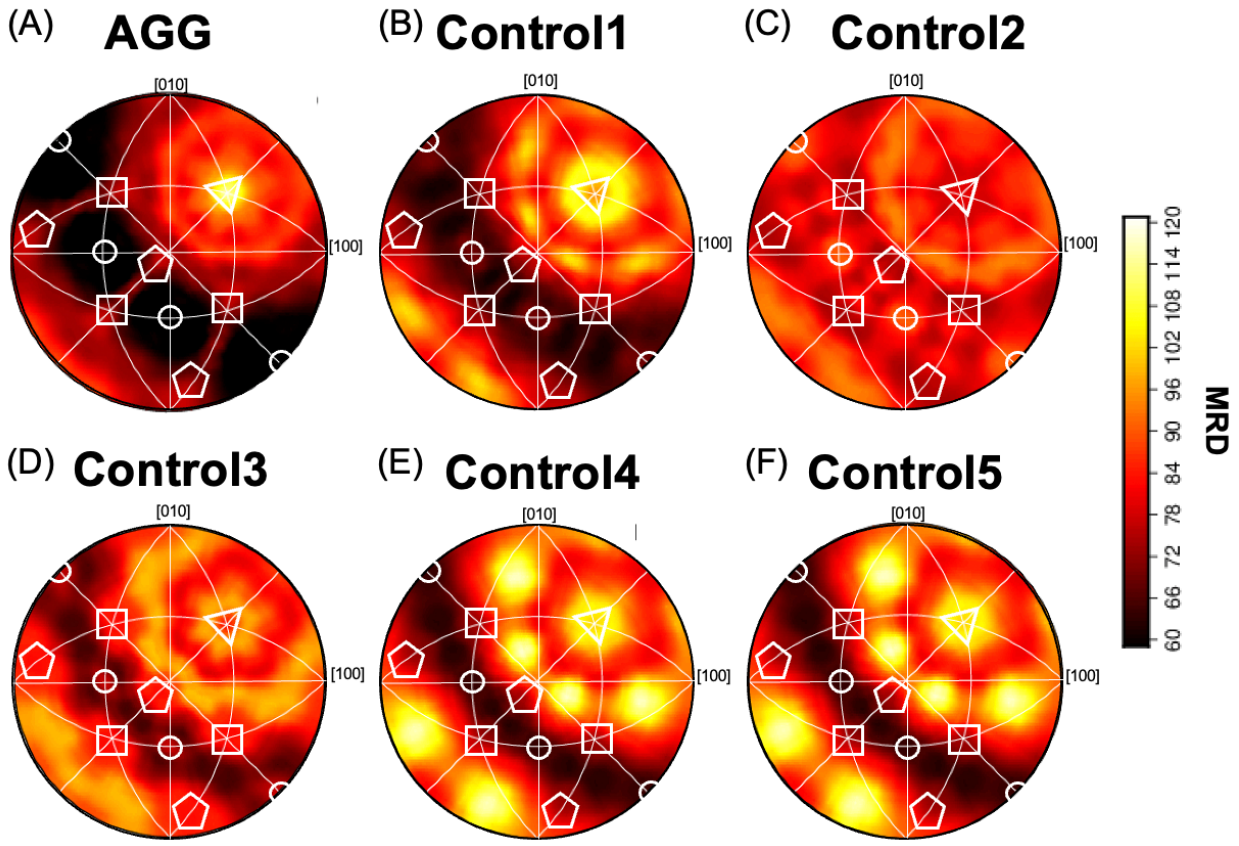


Figure S8: The relative populations (measured by multiple of random distribution, MRD) of Σ3 GBs associated with (A) abnormal grains and (B - F) each of the five control groups exhibiting NGG. All plots are stereographic projections along the [001] axis. The Σ3 GB plane inclinations indicated by triangles, circles, squares and pentagons are the (111), $(1\bar{1}0)$, $(\bar{1}11)$, and their complementary plane that is close to (100), respectively.